Charge transfer and excitation in $H^+ + CH_3$ collisions below 10 keV

Masatoshi Nagao, Ken-nosuke Hida, and Mineo Kimura
Graduate School of Sciences, Kyushu University, Fukuoka 812-8581, Japan

Sachchida N. Rai*
Computer Centre, Bijni Complex, North Eastern Hill University, Shillong 703003, Meghalaya, India

Heinz-Peter Liebermann and Robert J. Buenker
Fachbereich C-Mathematik und Naturwissenschaften, Bergische Universität Wuppertal, D-42119 Wuppertal, Germany

Hiroya Suno
Japan Agency for Marine-Earth Science and Technology, 3173-25 Showa-machi, Kanazawa-ku, Yokohama 236-0001, Japan

Phillip C. Stancil
Department of Physics and Astronomy and the Center for Simulational Physics, The University of Georgia, Athens, Georgia 30602, USA
(Received 2 April 2008; published 22 July 2008)

Charge transfer and electronic excitation in collisions of H^+ ions with CH_3 from a few tens of eV up to 10 keV are theoretically investigated. The adiabatic potential energy curves and corresponding wave functions are calculated by using the multireference single- and double-excitation configuration interaction method, and the scattering dynamics is studied based on the semiclassical impact parameter molecular-orbital close-coupling approach. Charge-transfer cross sections are found to be large and rather energy-dependent over the entire energy region studied. Electronic excitation is also energy-dependent with a sharp increase from below 10^{-17} to 10^{-16} cm^2. Most of the molecular products produced through charge transfer or excitation are known to be unstable and undergo fragmentation producing various hydrocarbon radical species. Hence, identification of fragmented species and their production mechanism are important for spectroscopic analysis.

DOI: 10.1103/PhysRevA.78.012708 PACS number(s): 34.50.−s

I. INTRODUCTION

Charge-transfer processes in collisions of ions with molecules from the high-eV to the low-keV energy regime, i.e., the intermediate energy region, have remained relatively unstudied both experimentally and theoretically, even though their importance is known in various applications from nanotechnology and medical physics to atmospheric science and astrochemistry as well as other areas of basic science [1]. One of the primary reasons for this lagging progress in atomic and molecular physics stems from inherent complexities in treating molecular targets in both theory and in experiment. Even for a relatively active research area such as chemical-reaction dynamics, the target species studied are very limited and collision energies considered are quite narrow, normally within the low-eV to meV region only. Despite such limited areas of study, however, based on our recent rigorous systematic investigations of ion-molecule collisions including those of the H_2 target [2–5], numerous new interesting findings and understanding emerge that undoubtedly help to revise our previous views of collision dynamics for molecular targets. These studies were partly stimulated by recent rapid developments in research areas such as fusion, plasma processing, and ion-beam technology. A proper theoretical understanding of dynamical aspects as well as the determination of cross-section estimates are urgently required in these applications.

We have initiated a series of rigorous theoretical studies of inelastic and electron capture processes in the collisions of H^+ ions with various molecules, primarily hydrocarbons, in the region below a few keV down to a few tens of eV. Hydrocarbon molecules are common molecular species under usual environmental conditions, and are found to exist abundantly in various astrophysical and atmospheric environments. They are particularly versatile for fusion reactors and plasma-chemistry atmospheres, which are known to play a crucial role in determining a number of physical effects [3]. Various kinds of hydrocarbons in sizable amounts have recently been found at the edge-plasma region in fusion reactors such as in divertors where carbon-faced materials are used, and the hydrocarbons produced are of concern since they play key roles as system contaminants in the reactor. Thus knowledge of such hydrocarbons and their fragmented species is crucial for description of the carbon chemistry in fusion research. Therefore, we also examine the fragmentation processes and fragmented species produced based on the calculated electronic states. In this series of research on hydrocarbons, we have undertaken the study of H^+-ion collisions with CH_4 [4], C_2H_2 [5], C_2H_4 [6,7], C_2H_6 [8], and CH_2 [9] in addition to C^+-ion collisions with C_3H_4 [10]. These investigations have unearthed various new insights and effects, and shown the importance of isotopic, isomeric, steric, and temperature effects, which previously were considered to be negligible in this collision energy domain. These findings have had a significant impact on various applications and

*Present address: Department of Physics, HMS Institute of Technology, Kyathsandra, Tumkur 572 104, Karnataka, India

have also stimulated careful reassessments of previous experimental studies.

In the present investigation as a part of the continuation of the molecular-target project, we report the results for electron capture and excitation in collisions of H^+ ions with CH_3 molecules between 60 eV and 10 keV. The methyl molecule, CH_3, is known to be highly reactive, but is also known to be produced as a radical and exist in such form in various astrophysical and atmospheric environments. It plays a key role in various molecular reactions in the universe and hydrocarbon technologies through its structural change mediator property. Furthermore, in ion-beam technologies such as etching, ion implantation, and surface modification, knowledge of structures and dynamics of hydrocarbon radicals is crucial for further development of basic sciences and technologies. Hence, we undertake the dynamical investigation of charge transfer in collisions of H^+ ions with CH_3 radicals below a few tens of keV, which is the energy range for most applications. The processes we are concerned with here are as follows:

$$\rightarrow \quad H + CH_3^{+} \text{ (charge transfer)}, \tag{1a}$$

$$H^+ + CH_3 \rightarrow H + CH_3^{+*} \text{ (charge transfer with target excitation)}, \tag{1b}$$

$$\rightarrow \quad H^+ + CH_3^{*} \text{ (target excitation)}. \tag{1c}$$

As described, most of the resulting ions and excited species after the collision are known to be unstable, and after a short lifetime they undergo fragmentation processes resulting in decomposition into smaller neutrals (radicals) and ions. Such radical cascades and secondary created ions are known to play a crucial role in biology, in environmental research, and in other fields. Therefore, it has been important to assess the production rates and yields of these radicals and ions, and to describe their mechanisms. We conduct the present study based on quantum chemical results for the electronic states and potentials of the CH_3 molecule.

II. THEORETICAL DESCRIPTION

A. Molecular states

The adiabatic potential-energy curves and corresponding wave functions are calculated by means of the multireference single- and double-excitation configuration interaction (MRD-CI) method [11–17], with configuration selection and energy extrapolation. The table CI algorithm [14,15] is employed for efficient handling of Hamiltonian matrix elements for the many-electron basis functions (symmetrized linear combinations of Slater determinants).

The atomic orbital (AO) basis set in the present calculations consists of contracted Cartesian Gaussian functions. For the carbon atom, a primitive basis $(10s,5p,2d,1f)$ contracted to $[4s,3p,2d,1f]$ due to Dunning [18] is employed. From the same reference, a primitive basis $(5s,2p,1d)$ contracted to $[3s,2p,1d]$ is used for the hydrogen atoms. Altogether the AO basis, therefore, consists of 95 contracted Gaussian functions.

The calculations are carried out in the C_{3v} and C_s point groups, with the electronic coordinate origin taken at the center of mass of the H^+-CH_3 complex. In the practical calculation of eigenvalues and eigenfunctions, all coordinates within the CH_3 molecule were frozen at the equilibrium intermolecular distances of the D_{3h} geometry [19]: $r_{C\text{-}H} = 1.079$ Å and the angle of H-C-H is 120°. One C-H bond is located on the positive side of the x axis with the C atom at the origin of the coordinate system, and the remaining two C-H bonds elongate in the xy plane on the negative side of the x axis. We have considered three different molecular configurations: (i) the proton approaches the carbon atom in the center of the molecule perpendicular to the molecular plane on the z axis, (ii) the proton approaches one of the hydrogen atoms in the molecular plane along the x axis, and (iii) the proton approaches carbon in the molecular plane along the x axis, as shown in Figs. 1(a)–1(c). These three collision orientations were chosen as they are believed to adequately sample the full Jacobi angular (θ,ϕ) parameter space and are also representative of the main interaction configurations.

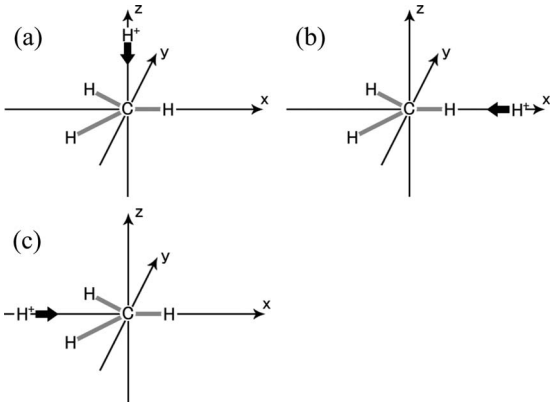

FIG. 1. (a)–(c) Schematic diagram indicating the molecular axis orientation employed for the $[H+CH_3]^+$ collision system for cases (i)–(iii). Case (i) represents the perpendicular impact onto the molecular plane, while cases (ii) and (iii) have the proton approaching the carbon atom in the molecular plane toward one of the hydrogen atoms, or in their center.

The target molecular geometry is fixed at the equilibrium conformation of the neutral ground state during the collisions. This restriction is justified since the present collision time is much shorter, less than 10^{-17} s, than the relaxation time of 10^{-13} s or longer. Hence, only the internuclear distance R between the H^+ projectile and the carbon atom was varied in the molecular-state calculations.

B. Scattering dynamics

In the semiclassical impact parameter molecular-orbital close-coupling (MOCC) method [20], the relative motion of the projectile nucleus is treated classically with a straight-line trajectory, while the electronic motion is treated quantum mechanically. The total wave function for this collision system is expanded in terms of products of molecular states and electron translation factors (ETFs). The ETF ensures that the asymptotic scattering condition is satisfied. Substituting the total wave function into the time-dependent Schrödinger equation, we obtain coupled equations as a function of time,

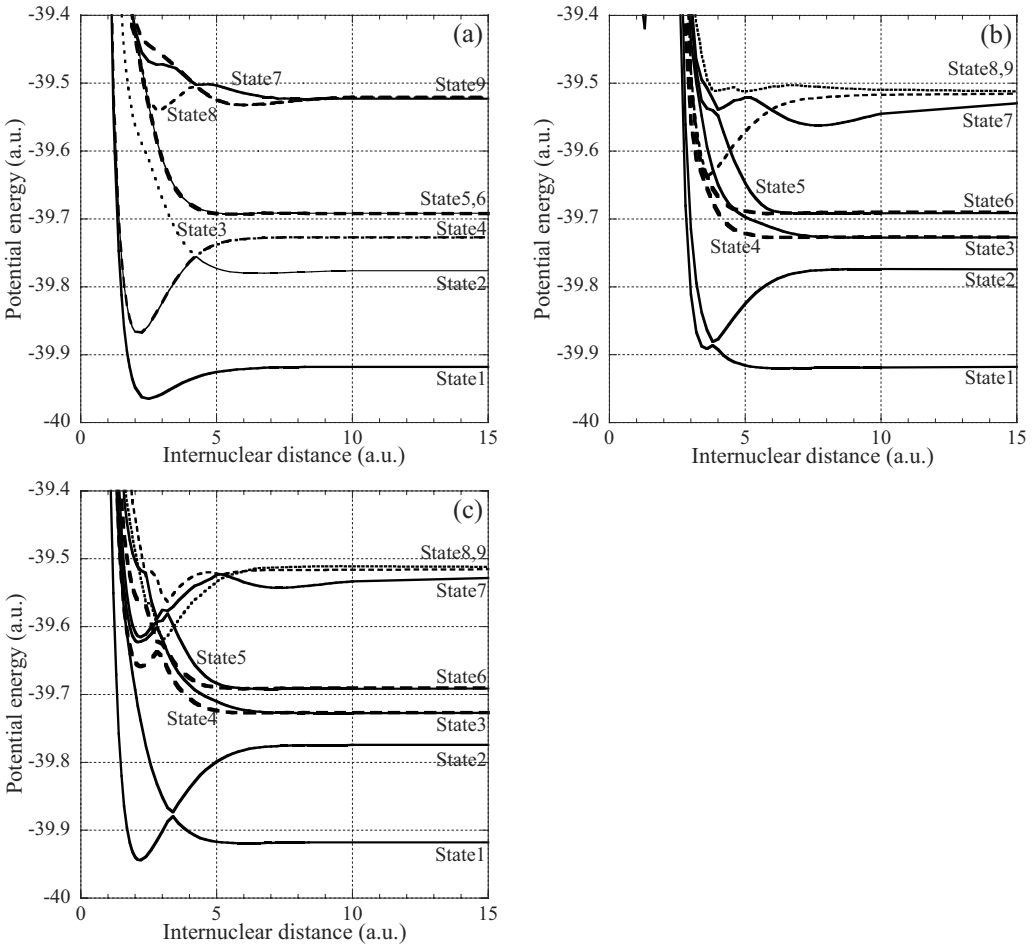

FIG. 2. (a)–(c) The adiabatic potentials of the $[H+CH_3]^+$ system. (i) The proton approaches the carbon atom perpendicular to the molecular plane, (ii) the proton approaches one of the hydrogen atoms in the molecular plane along the x axis, and (iii) the proton approaches the carbon atom in the molecular plane from the $-x$ direction. (a)–(c) are for cases (i)–(iii), respectively.

and all radial and rotational coupling matrix elements among molecular states considered are included in the present calculations. The transition amplitudes can be obtained by solving the coupled equations. By integration of the square of those transition amplitudes over impact parameter, the cross sections can be determined.

In the present calculations, we have carried out up to nine-state close-coupling treatments. The corresponding molecular states arise from the initial $[H^+ + CH_3]$, the charge transfer $[H+CH_3^+]$, the target excitation $[H^+ + CH_3^*]$, and the charge transfer with excitation $[H+CH_3^{+*}]$ channels.

The impact parameter step size, Δb, and maximum impact parameter b_{max}, were varied to ensure convergence of the cross sections. As an example, at 1 keV we found that $\Delta b = 0.5$ a.u. and $b_{max} = 15.0$ a.u. were sufficient to obtain convergence. As all calculations include a total of nine electronic channels, we did not test the electronic basis-set convergence.

III. RESULTS AND DISCUSSION

We first discuss some features of molecular structures and couplings, followed by our results on scattering dynamics.

A. Adiabatic potentials and corresponding couplings

The adiabatic potentials of the $[H+CH_3]^+$ system for the cases (i), (ii), and (iii) are shown in Figs. 2(a)–2(c). In all figures, the nine molecular states are shown that are actually employed in the present scattering calculations. All states are enumerated with increasing energy from the lowest. Notice that the asymptotes for the various channels are the same in each case since they correspond to the same separated fragments.

For cases (i)–(iii), state 2 corresponds to the initial state, i.e., the $[H^+ + CH_3]$ channel. State 1 is the ground charge-transfer $[H+CH_3^+]$ state, while states 3–6 are the charge-transfer plus electronic excitation $[H+CH_3^{+*}]$ states. States 7–9 correspond to the target electronic excitation $[H^+ + CH_3^*]$ states. States 3–6 are doubly degenerate states that possess σ- and π-type features.

There are some distinctive characteristics in the three cases. It is apparent that for (i), very weak (or no) avoided crossings can be observed among the states except between 2 and 3, while for (ii), intermediately strong avoided crossings emerge between state 1 and 2, but no other strong couplings are seen among the low-lying states until one reaches state 7 and higher, where strong mixings do occur. For (iii), very

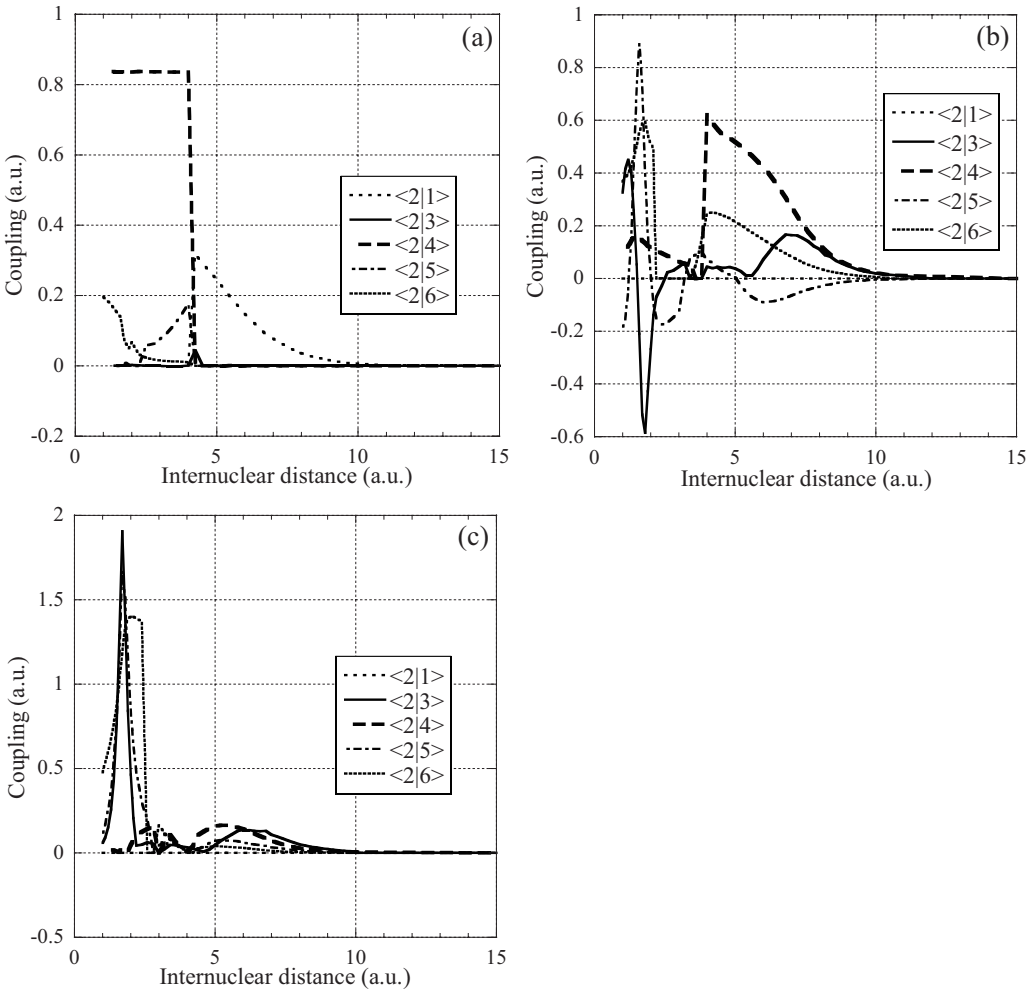

FIG. 3. (a)–(c) Representative radial couplings between the initial state (state 2) and the charge-transfer states for cases (i), (ii), and (iii), respectively.

strongly avoided crossings are seen among various states, which is remarkably different from the preceding two cases. In summary, the amount of mixing is weak in (i), intermediate in (ii), and strong in (iii). This clearly suggests quite different dynamics in all three cases, and hence a very strong steric effect can be expected for the charge transfer and excitation dynamics. The shape of the lowest energy curve in each case ties closely with space configuration and exhibits gradual attractive or repulsive integration modes of the impacting proton into an off-equilibrium CH_4^+ collision intermediary.

Next, we examine the corresponding radial couplings for the three cases, as shown in Figs. 3(a)–3(c), to highlight their differences and similarities in order to have a better insight into the resulting dynamics. Here couplings between the initial state and charge-transfer states with target excitation are included. For case (i), a broad peak between state 2 (the initial state) and state 4 can be observed, since these adiabatic potentials are close to one another in the region of 1–4 a.u. For case (ii), although state 1 and the initial state have an avoided crossing at an internuclear distance around 3.8 a.u., the maximum value of the coupling is found to be only about 0.002 a.u., and hence it is not as strong as perhaps might be expected. This is, in fact, consistent with the short-range shoulder on the left and small energy separation of states 1 and 2 at lower R. Couplings between the initial state and state 4 possess a large and broad peak around 6–7 a.u. Hence, these couplings are expected to play important roles for the flux exit to higher levels via slowly occurring delocalized transitions.

For case (iii), state 1 and the initial state have a very strong avoided crossing near 3.4 a.u. as seen above, but the local value of the coupling is about 0.11 a.u., which is still regarded as weak. The $\langle 2|3\rangle$ and $\langle 2|5\rangle$ couplings are generally found to be much sharper than those of $\langle 2|4\rangle$ and $\langle 2|6\rangle$ at short distances with stronger internuclear repulsion. Other couplings of significance connect with excited states and are very strong. Most of those have large peaks at internuclear separations beyond 2–4 a.u., and the location moves out to larger distances as the excitation of the level increases. Therefore, the ladder-climbing mechanism plays an important role here for flux promotion. This is a characteristic feature in this case, and is likely to lead to significantly greater charge transfer to the excited states compared to the other two cases.

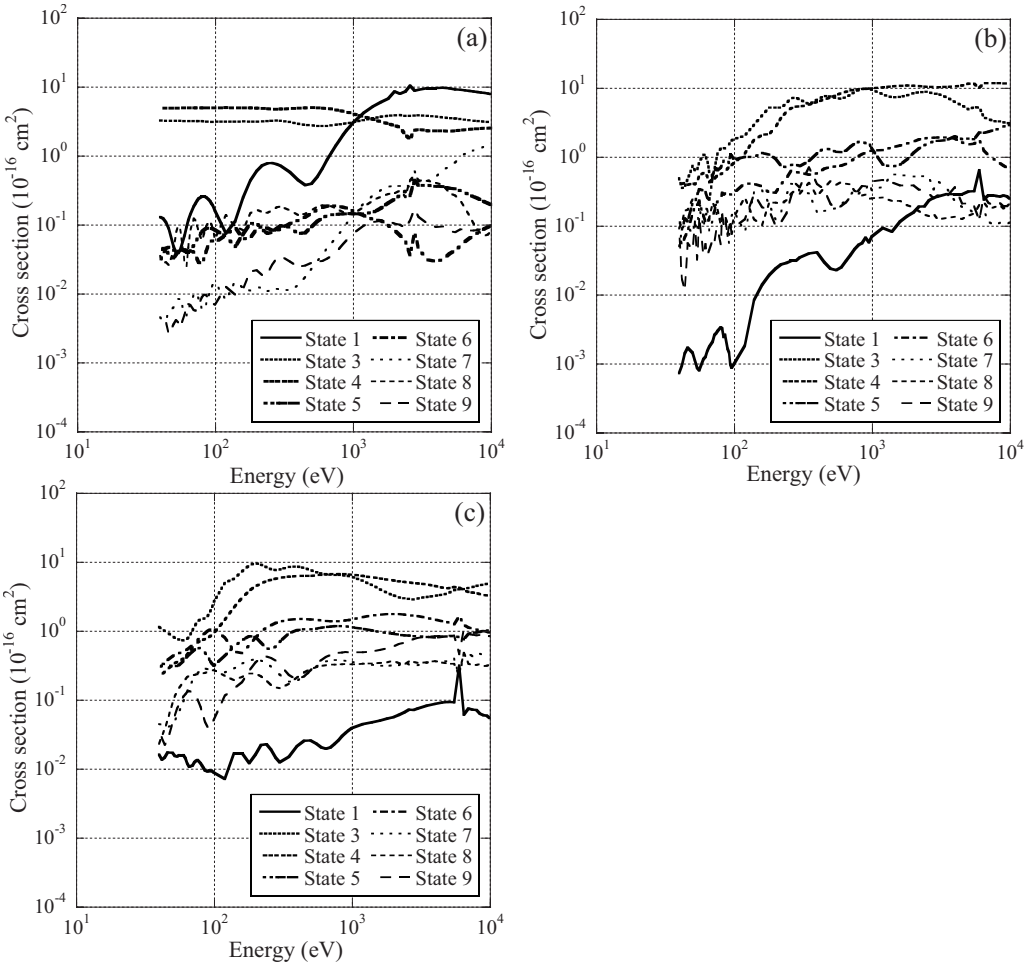

FIG. 4. (a)–(c) Partial cross sections for each channel for cases (i), (ii), and (iii), respectively, where state 2 [H^++CH_3] is the initial channel.

B. Partial cross sections for each individual level

Calculated partial cross sections for the cases (i), (ii), and (iii) are shown in Figs. 4(a)–4(c). For case (i), the partial cross section to state 4 is the largest among all channels throughout most of the considered energy range, except to state 1 at the highest energy. This may be due to a large, broad coupling peak connecting the two states [see Fig. 2(a)]. The excitation cross section for transitions to states 7 and 9 is found to be very small at the lowest energy, although it begins to become sizable as the energy increases. The charge transfer to state 1 (the ground state) is found to be small at low energies, but as the energy increases, it quickly becomes the dominant contributor above 1000 eV or so. Partial cross sections to states 5, 6, and 8 are found to be close in magnitude. This can be expected from weak couplings between the initial state 2 and each of these states. Since all channels interfere strongly, partial cross sections show rapid oscillations, some in-phase and others out-of-phase, suggesting constructive or destructive interferences in any energy domain.

For case (ii), the partial cross sections to states 3 and 4 are found to dominate the inelastic scattering. Partial cross sections for states 5–9 are seen to be very close in magnitude below ~1 keV, but they all interfere very strongly, which translates to cross-section in-phase and out-of-phase oscillations due to strong couplings among these states. This strong mixing among high-lying states suggests that it is necessary to take many higher states into consideration in the calculation, particularly at high energy. One significant aspect is different from case (i), namely the charge-transfer cross section to the ground state has become much smaller than those of transfer plus target excitation of states 3 and 4 and 5 and 6. Even though the potentials of the initial state and the ground state have an avoided crossing around 3.8 a.u., the coupling between the two states is weak as described above, and consequently this feature makes the partial cross section of the ground state rather small. Target excitations in states 7–9 are small and well mixed with charge transfer in high-lying states.

For case (iii), states 3 and 4 are responsible for the dominant contribution to charge transfer. These two states are strong contributors in the entire energy region. All the rest show similar cross sections and strong interferences for each state, and the in-phase and out-of-phase oscillatory structures are well visible. Target excitations in states 7–9 are also important and are well mixed with those of high-lying charge transfer. The energy dependence in all partial cross sections

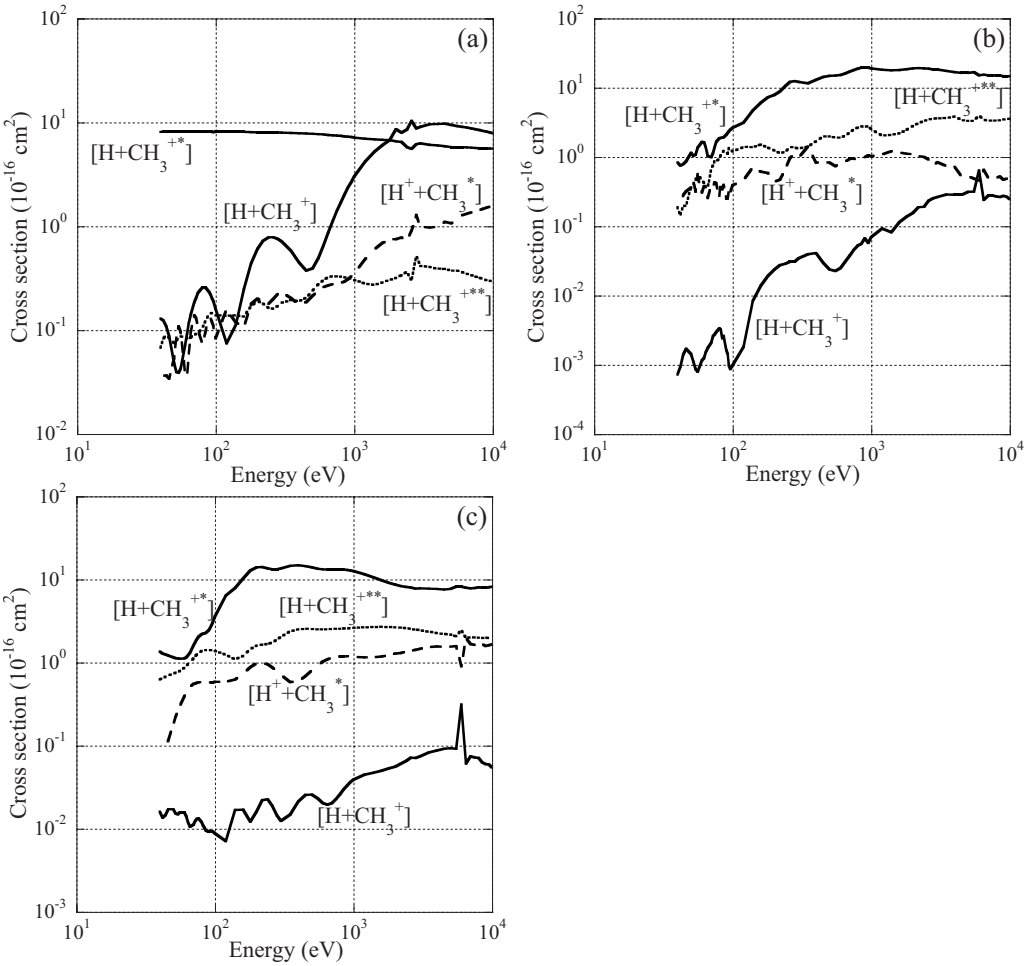

FIG. 5. (a)–(c) Partial cross sections for each manifold for cases (i), (ii), and (iii), respectively. Each curve is labeled by its asymptotic designation for the final channel, while the initial channel is $[H^+ + CH_3]$.

in case (iii) is found to be rather weak compared to cases (i) and (ii), which show a conspicuous energy dependence. In other words, the denser network of active transition regions for this case smooths out the energy dependence of individual transition probability functions more efficiently.

As a whole, a very strong configuration dependence for individual processes is apparent and the molecular orientation (steric) effect is significant. In all cases, charge transfer to states 3 and 4 is dominant, while in case (i), transitions to state 1 are the most significant in the high-energy region. There are resonancelike structures in the cross sections near 2.8 keV for case (i) and in the vicinity of 6 keV for cases (ii) and (iii). These are found to correlate with significant increases in the charge-transfer probability for small impact parameters.

Numerical features can be observed in Figs. 4(b) and 4(c) for capture cross sections to the ground state at intermediate keV collision energies. These features occur when the fixed accuracy of the integration algorithm numerically is nearly equal to the ratio of the energy separation between two lowest-energy curves at a mutual crossing region per kinetic energy of an impacting proton. Such a limited irregular feature is consistent with the present numerical procedure, and is therefore kept as an illustration of the implied theoretical error, typically in the weakest product channel, and is perhaps analogous to experimental uncertainty. Therefore, for collision energies near 6 keV, a smooth interpolated cross section is appropriate while at lower energies the observed oscillatory structures are deemed to be physical.

C. Partial cross sections for each manifold at each molecular configuration

Figures 5(a)–5(c) present calculated partial cross sections summed for each process in Eq. (1) for cases (i), (ii), and (iii). In these figures, $[H+CH_3^+]$ corresponds to the charge-transfer process to the ground state, and $[H+CH_3^{+**}]$ to the charge-transfer process to the first excited state. $[H+CH_3^{+***}]$ designates that process to the group of three excited states lying energetically higher than that of $[H+CH_3^{+**}]$. Finally, $[H^+ + CH_3^*]$ represents target excitation.

For case (i), the partial cross section for $[H+CH_3^{+*}]$ formation is the largest for the lower energy region, and is found to be larger than those for the other processes by a factor of 2 or more. Cross-section values for $[H+CH_3^+]$ have a conspicuous energy dependence, and they are the largest in the region of higher energy. Cross-section values for the

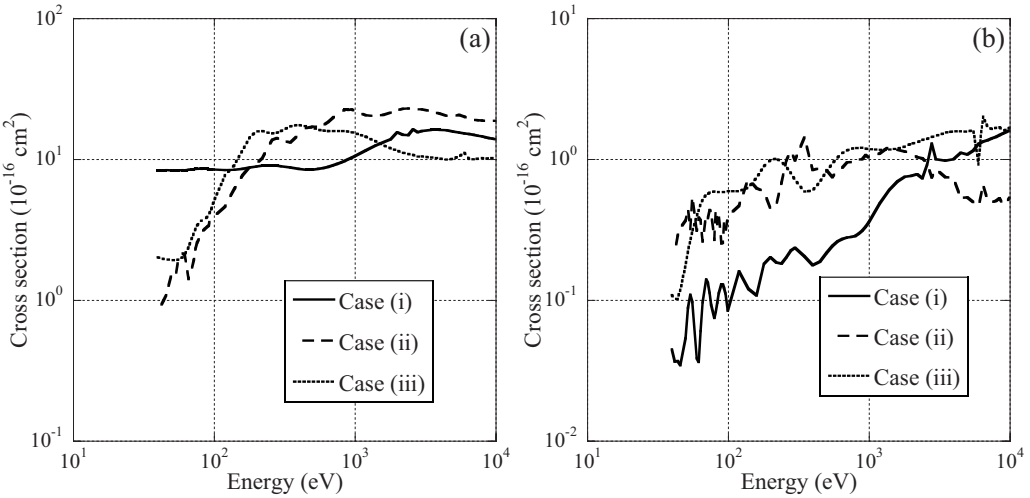

FIG. 6. Total charge transfer and electronic excitation cross sections for each molecular configuration: (a) for charge transfer and (b) for excitation for H^+ collisions with CH_3.

$[H+CH_3^+]$, $[H+CH_3^{+**}]$, and $[H^++CH_3^*]$ formations are found to oscillate rather strongly due primarily to interferences. It is interesting to note that cross sections for transitions to $[H+CH_3^+]$ and $[H^++CH_3^*]$ also display both in-phase and out-of-phase oscillatory structures depending on the energy region, suggesting a strong and sensitive coupling scheme between the two levels.

For case (ii), the partial cross section for $[H+CH_3^{+*}]$ formation is the largest over the whole energy region, and that for the $[H+CH_3^+]$ formation is found to be the smallest. The cross-section values for the $[H+CH_3^{+**}]$ and $[H^++CH_3^*]$ formations are similar in magnitude and in energy dependence at all considered energies, suggesting strong mixing between these manifolds. For case (iii), the partial cross section for $[H+CH_3^{+*}]$ formation is found to be the largest. The partial cross sections for the $[H+CH_3^+]$ and $[H+CH_3^{+**}]$ formations show quite different features from those for the other molecular configurations, that is, except for the oscillations, they are rather flat with increasing energy.

Except for case (i), formation of the ground state ($[H+CH_3^+]$) is rather insignificant. This is an important observation and we will return to this point when discussing the comparison with empirical scaling predictions. For all the molecular configurations, the $[H+CH_3^{+*}]$ formation is the most important. It is clear that a very strong dependence for charge transfer and excitation on molecular configuration occurs.

D. Charge transfer and excitation summed over all channels

Total charge-transfer cross sections and those for excitation in the collision energy range between 60 eV and 10 keV for each molecular configuration are shown in Figs. 6(a) and 6(b), respectively. The results for the charge transfer shown are a sum of all states corresponding to the asymptotes of $[H+CH_3^+]$, $[H+CH_3^{+**}]$, and $[H+CH_3^{+**}]$, while that of excitation is for the asymptotic state of $[H^++CH_3^*]$ only, as described in Sec. III A. The total charge-transfer cross sections show very different features depending on the molecular configuration. For instance, those for case (i) are seen to decrease rather smoothly with decreasing energy, while those for cases (ii) and (iii) show much stronger oscillatory structures suggesting strong interference among all states involved. These features can be understood from our previous discussion in Sec. III B. For cases (ii) and (iii), the energy dependency of the charge-transfer cross section is strong, in particular at low energy. In Fig. 6(b), all three target excitation cross sections are energy-dependent and oscillate strongly. They are also greatly different depending on molecular configuration. For all molecular configurations, the charge-transfer cross sections are a factor of 2 or more larger than those for target excitation.

E. Comparison with other results

Since there are no experimental or other theoretical studies for this collision system, we make a comparison with results derived from a scaling relation. Figure 7 compares our present results obtained by averaging over the three geo-

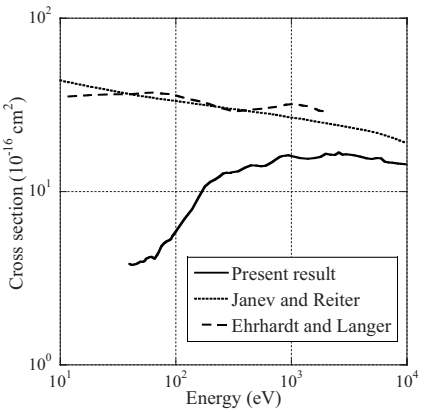

FIG. 7. Comparison of the present charge-transfer cross sections with those of Janev and Reiter [21] and Ehrhardt and Langer [22] for H^+ collisions with CH_3.

metrical conformations, as illustrated in Fig. 6(a), with the theoretical predictions by Janev and Reiter [21] and Ehrhardt and Langer [22]. Janev and Reiter proposed a scaling law to predict cross-section data for electron and proton impacts on CH_y ($y=1-4$) and CH_y^+ molecular species, based on the perturbative analytical approach, and provided a complete set of charge-transfer cross sections for these molecular targets. Ehrhardt and Langer also made corresponding recommendations. As is apparent, Janev and Reiter have predicted a slowly increasing trend with decreasing energy. While the present result is in good accord with their expectations from about 2 keV and above, it begins to depart from them below 1 keV, with a sharp decrease having been computed below ~600 eV. This energy dependence at lower energies is a marked difference between the three results. This feature in the present results is typical for an endothermic reaction, while that of Janev and Reiter is more representative of an exothermic one. As in Figs. 2(a)–2(c) in the adiabatic potentials, a sharp avoided crossing has been found connecting the initial (state 2) and the ground charge-transfer state 1. As is apparent from Figs. 5(a)–5(c), however, this crossing is found to play a secondary role for the charge-transfer dynamics, hence being more endothermic in nature as a whole. At the lowest energy studied at 50 eV, the difference between the two results is found to be approximately an order of magnitude. Since the procedure used by Janev and Reiter to derive the analytical expression is based on a simple perturbative approach, their formula may not be fully appropriate, particularly in the low-energy domain. For capture to the CH_3^+ electronic ground state, transitions to the lowest vibrational state are likely to dominate at the highest considered energies, but for energies between 10 and ~100 eV, transitions to higher vibrational states may give larger cross sections, particularly those in near resonance. From Figs. 2(a)–2(c), the energy gap between states 1 and 2 is about 4.1 eV. However, the dissociation energy of the CH_3^+ electronic ground state is about 5.5 eV (for $CH_2^+ + H$). Therefore, there will likely be a significant number of CH_3^+ (+H) vibrational states in near resonance with the entrance channel $[H^+ + CH_3]$. The importance of capture to CH_3^+ ($\nu > 0$) will depend on a complicated interplay of asymptotic energy gap (an exponential energy gap law) and coupling strength. Based on pure energetics, capture to highly excited vibrational states (but exoergic) will dominate, but since the coupling between electronic states 1 and 2 appears weak, the coupling magnitude may suppress this. The true answer for $[H^+ + CH_3]$ is probably confined among the three curves shown in Fig. 7, with the Janev and Reiter prediction tied to the above motivated mechanism. It is certainly an upper limit, while our result for $E \geqslant 200-300$ eV can be considered a lower bound since the vibrational motion of the molecular product is not considered in the current work.

F. Fragmentation

Although no rigorous study of fragmentation mechanisms and the resulting fragmented species of CH_3 radicals upon proton impact was carried out in the present study, it is quite important to overview possible consequences of such a mechanism for various applications. For fusion, for example, spatial energy distributions of fragmented C, CH, CH_2, and H_2 species grossly alter plasma distribution and temperature. So we give here some qualitative arguments about these processes. There are a number of fragmentations that can occur as a result of collisions of a methyl radical with H^+ ions. The dissociation energy of CH_3 itself (along a CH bond) is thought to be at most 4.9 eV. The CH_2 product (methylene) is known to possess a $^3B_1$ ground state with a bond angle of 134 deg. It has a low-lying $^1A_1$ state with a bond angle of 104 deg, however with an excitation energy of only 0.37 eV. The ground state D_e value for the methylene radical is believed to be in excess of 4.23 eV. The CH diatomic fragment has a $^2\Pi$ ground state and a $^4\Sigma^-$ excited state lying 0.75 eV above it. The ground state dissociates directly into $C(^3P) + H(^2S)$ ground-state products of the atoms. The corresponding D_e value is 3.60 eV, so this bond is notably weaker than for either CH_3 or CH_2. Therefore, electronic target excitation to $[H^+ + CH_3^*]$, Eq. (1b), will likely result into fragmentation species CH_2, CH, C, and H. As a result of CH_3^+ dissociation [23], C^+, CH^+, CH_2, CH_2^+, H, H^+, H_2, and H_2^+ species are obtained following charge transfer and excitation to $[H + CH_3^{+*}]$, Eq. (1c).

IV. SUMMARY AND CONCLUSIONS

Charge transfer and electronic excitation processes in collisions of H^+ ions with CH_3 molecules between a few tens of eV up to 10 keV have been investigated theoretically. Charge-transfer cross sections in the present calculation are energy-dependent in nature. Target electronic excitation cross sections sharply increase as the energy increases. The present results are somewhat different from those of Janev and Reiter, who derived analytical formulas to represent charge-transfer cross sections for various hydrocarbon molecules based on a truncated perturbative scheme. In view of their simplicity, this disagreement is not unexpected, though the current results are only applicable to the lowest vibrational state of the product ion. The present cross-section data should be useful for a variety of applications.

ACKNOWLEDGMENTS

This work was supported in part by the Ministry of Education, Science, Sport, Culture and Technology, the National Institute for Fusion Science, a research project by the Foundation for Promotion of Material, Science and Technology (K.H. and M.K.), Grant No. BU 450/7-3 from Deutsche Forschungsgemeinschaft (H.P.L., S.N.R., and R.J.B.), and NASA Grant No. NNG05GD98G (P.C.S.).

[1] E. W. McDaniel, J. B. A. Mitchell, and M. E. Rudd, *Atomic Collisions* (Wiley Interscience, New York, 1993).
[2] B. H. Bransden and C. J. Joachain, *Ion-Atom Collisions* (Oxford University Press, New York, 1993).
[3] H. Tawara, Y. Itikawa, H. Nishimura, H. Tanaka, and Y. Nakamura, At. Plasma-Mater. Interact. Data Fusion **2**, 41 (1992).
[4] M. Kimura, Y. Li, G. Hirsch, and R. J. Buenker, Phys. Rev. A **52**, 1196 (1995).
[5] M. Kimura, Y. Li, G. Hirsch, and R. J. Buenker, Phys. Rev. A **54**, 5019 (1996).
[6] R. Suzuki, S. N. Rai, H.-P. Liebermann, R. J. Buenker, L. Pichl, and M. Kimura, Phys. Rev. A **71**, 032710 (2005).
[7] T. Kusakabe, K. Asahina, A. Iida, Y. Tanaka, Y. Li, G. Hirsch, R. J. Buenker, M. Kimura, H. Tawara, and Y. Nakai, Phys. Rev. A **62**, 062715 (2000).
[8] R. Suzuki, S. N. Rai, H.-P. Liebermann, R. J. Buenker, L. Pichl, and M. Kimura, Phys. Rev. A **72**, 052710 (2005).
[9] H. Suno, S. N. Rai, H.-P. Liebermann, R. J. Buenker, M. Kimura, and R. K. Janev, Phys. Rev. A **70**, 032703 (2004).
[10] T. Kusakabe, K. Asahina, J. P. Gu, G. Hirsch, R. J. Buenker, M. Kimura, H. Tawara, and Y. Nakai, Phys. Rev. A **62**, 062714 (2000).
[11] R. J. Buenker and S. D. Peyerimhoff, Theor. Chim. Acta **35**, 33 (1974).
[12] R. J. Buenker and S. D. Peyerimhoff, Theor. Chim. Acta **39**, 217 (1975).
[13] R. J. Buenker, Int. J. Quantum Chem. **29**, 435 (1986).
[14] R. J. Buenker, in *Proceedings of the Workshop on Quantum Chemistry and Molecular Physics, Wollongong, Australia*, edited by P. Burton (University Press, Wollongong, 1980), p. 1.5.1; R. J. Buenker, in *Current Aspects of Quantum Chemistry*, edited by R. Carbo (Elsevier, Amsterdam, 1982), Vol. 21, p. 17; R. J. Buenker and R. A. Phillips, J. Mol. Struct.: THEOCHEM **123**, 291 (1985).
[15] S. Krebs and R. J. Buenker, J. Chem. Phys. **103**, 5613 (1995).
[16] R. J. Buenker, D. B. Knowles, S. N. Rai, G. Hirsch, K. Bhamuprakash, and J. R. Alvarez-Collado, in *Studies in Physical and Theoretical Chemistry*, edited by R. Carbo (Elsevier, Amsterdam, 1989), Vol. 62, p. 181.
[17] D. B. Knowles, J. R. Alvarez-Collado, G. Hirsch, and R. J. Buenker, J. Chem. Phys. **92**, 585 (1990).
[18] T. H. Dunning, Jr., J. Chem. Phys. **98**, 1007 (1989).
[19] G. Herzberg, *Molecular Spectra and Molecular Structure* (Van Nostrand Reinhold, New York, 1966), Vol. III, p. 609.
[20] M. Kimura and N. F. Lane, Adv. At., Mol., Opt. Phys. **26**, 79 (1990).
[21] R. K. Janev and D. Reiter, Phys. Plasmas **9**, 4071 (2002).
[22] A. B. Ehrhardt and W. D. Langer, Rep. PPPL-2477, Princeton Plasma Phys. Lab., Princeton, NJ (1986).
[23] R. J. Blint, R. F. Marshall, and W. D. Watson, Astrophys. J. **206**, 627 (1976).